International Journal of Heat and Technology
Vol. 42, No. 5, October, 2024, pp. 1559-1566
Journal homepage: http://iieta.org/journals/ijht

Investigating Thermal Control Methods for Lithium-Based Batteries Utilizing Metal Foams Saturated with Air

Aanandsundar Arumugam[1*], Bernardo Buonomo[1], Ulavathi S. Mahabaleshwar[2], Oronzio Manca[1]

[1] Department of Engineering, University of Campania "Luigi Vanvitelli", Aversa 81031, Italy
[2] Department of Studies in Mathematics, Davangere University, Shivagangotri 577007, India

Corresponding Author Email: aanandsundar.arumugam@unicampania.it

https://doi.org/10.18280/ijht.420509

Received: 16 June 2024
Revised: 7 August 2024
Accepted: 22 August 2024
Available online: 31 October 2024

Keywords:
battery thermal management systems, electric vehicles, finite volume analysis, generalized reduced gradient algorithm, lithium-based batteries, metal foam

ABSTRACT

Lithium-based battery packs consist of numerous battery cells which form an essential component of electric vehicles. Inadequate heat transfer creates various challenges to safety issues in these batteries. Hence, assessment of the thermal performance of battery packs is an integral part of the design phase. In this study, a numerical approach of the system is implemented using a three-dimensional cylindrical model of a lithium Manganese dioxide battery cell. The model incorporates the application of the metal foam of different geometrical parameters saturated with air for the thermal cooling of batteries. The model considers the cooling phenomenon during discharge process of a cell with a C-rate of 1C respectively. The change in internal resistance of the cell with temperature during the process is estimated using the Generalized Reduced Gradient (GRG) algorithm. The system is considered to be adiabatic by maintaining a flow of liquid through convective tubes, to maintain a constant temperature. The Battery Thermal Management System design is proposed using the Ansys-Fluent software assuming finite volume analysis. The results are analyzed in terms of the maximum battery temperature attained and with the maximum surface temperature of the battery and the metal foams acquired during the process.

1. INTRODUCTION

Over the past few decades, the primary sources for electricity generation were conventional, including fossil fuels and nuclear energy. However, the growing environmental concerns and a significant escalation in fossil fuel costs driven by the global energy demands have accelerated the transition towards renewable energy. The integration of sustainable energy sources into the electricity networks reduces the threats and hazards imposed by the effects of climate change, global warming, and pollution [1].

Electric Vehicles (EVs) are emerging as a preferable alternative to conventional engine-powered vehicles, thereby offering several benefits including the decreased emissions of harmful toxic gases thus contributing to a cleaner and sustainable environment. The utilization and storage of the non-conventional energy resources in batteries have minimal impacts on climate and ecosystems. The EVs are gaining much attraction due to their significant features such as fewer moving parts, reduced greenhouse gases emissions, lower maintenance costs, resilience to climate change and supports conservation of biodiversity [2].

Generally, all batteries are comprised of a positive electrode termed as the cathode and a negative electrode termed as anode and an ionic electrolyte. A few batteries also include a separator to maintain electrode isolation during the process of ion transfer. These elements constitute a single cell arrangement. The batteries are also categorized as wet cells with liquid electrolytes or dry cells with gel or solid electrolyte. Multiple cells are stacked together and enclosed in order to form a battery arrangement [3].

The lithium-ion cell, invented in 1979, uses lithium as an ion rather than a metal effectively resolves issues related to dendrite growth during the process of recharging. The battery cell offers an open-circuit voltage of 4V. Moreover, the battery's performance suffers when subjected to excessive heat generation phenomenon during the process of excessive heating leading to capacity degradation. Additionally, lithium-based batteries are quite popular due to their relatively low self-discharge rate, higher energy and power density and absence of memory effect. The battery's life cycle is generally improved by minimizing the depth of discharge and avoiding full charging. Considering the cost analysis, lithium-ion technology finds primary applications in consumer electronics and is relatively integrated into vehicles and high-power applications [3, 4].

These batteries incur high costs primarily due to cobalt and nickel usage, prompting the exploration of substitutes. Manganese has been examined to be a better substitute, with uncertainties in stability indicating issues of charge capacity losses and chemical instability. Recent advancements have indicated improvements in the chemical structure analysis. However, the performance degrades as the temperature reaches elevated levels. Recent studies demonstrate the

application of aluminum-silicon-graphite anodes to improve energy density and safety issues. Silicon has been observed to indicate relatively better energy capacity and reduction in cell degradation from internal mechanisms [4, 5].

The lithium-ion based batteries are relatively better in performance in comparison with various other chemistries. The essential characteristics of the lithium-ion based batteries with their counterparts is described with respect to various characteristics. The lithium-based batteries generally tend to have relatively higher specific energy ranging from 80-180 Wh/kg as compared to Nickel metal hydride which has a value of around 60-80 Wh/kg and Nickel cadmium batteries having a value of 30-60 Wh/kg. Lead-acid batteries have the lowest values ranging from 35-50 Wh/kg. The self-discharge rate of lithium-based batteries are 2-10%/month, as compared to 15-25% and 5-15%/month in case of Nickel compositions. Nickel cadmium batteries generally have a longer life span of around 10-15 years as compared to lithium-ion which has a life span of around 5years which is almost the same in the case of Lead-acid batteries. The specific power of lithium-based batteries is relatively too high in the range of 200-1000 W/kg. Nickel cadmium batteries possess the lowest specific power which ranges from 80-150 W/kg followed by nickel metal hydride and lead extending from 200-300 and 150-400 W/kg respectively. The cell voltage of lithium batteries usually ranges from 3.05-4.2 V, where 4.2 V is the maximum voltage. The nominal voltage of the lithium-based batteries is usually 3.6 V. On the other hand, the cell voltages of lead-acid batteries extend to 2.1V, whereas the voltages of nickel-based batteries are 1.2V respectively. The maximum Depth of Discharge (DOD) of lithium-based batteries is usually 100%, whereas Nickel cadmium extends up to 80% and lead acid extends from 20 to 80% [3, 4, 6].

Temperature impacts on batteries are broadly classified into two categories namely the impacts during low temperatures and impacts during high temperatures. Inadequate temperature control results in unanticipated performance decreases leading to a phenomenon termed as the ‘Thermal Runaway’. In order to effectively utilize the lithium-based batteries and to unlock its benefits a Battery Thermal Management Systems (BTMS) is required to be employed. The BTMS is generally designed to ensure optimal temperatures and uniform temperature distribution across the cells in a battery pack system [7]. BTMS prioritizes the modeling of battery cells due to its pivotal role. It has an essential role to play due to analyzing the battery performance across diverse operating conditions, which in turn facilitates the development of more effective BTMS designs. Given the inherent nonlinear nature of battery behavior, the design of an optimal Battery Management System is mandatory. Numerous models have been devised, taking into account battery characteristics such as temperature, charge/discharge cycles, State of Charge (SOC), and capacity degradation dynamics. Multifunctional Battery Management System are commonly utilized to forecast and analyze battery issues at different stages, from individual cells to entire packs comprising multiple modules. These systems ensure efficient cell operation by facilitating proper communication among modules during operation. Effective thermal management is essential for maintaining optimal operating temperatures in Battery Management Systems, which aids in controlling the excessive heat buildup and preventing the occurrence of thermal runaway. Generally various cooling techniques have been adopted for this purpose [7, 8].

The conventional Battery Thermal Management System is divided into two main categories namely the active cooling mechanism and the passive cooling mechanisms. Active cooling mechanisms include air cooling, heat pipe cooling and fluid cooling which dissipates heat from the battery pack using air or liquid. Conversely, passive cooling involves phase change materials (PCM) cooling, which is preferred over air and liquid cooling systems due to its elimination of electrical and mechanical components such as fans, pumps, and connections. The adoption of PCMs for passive thermal management in lithium-based battery technologies has increased in recent years. As a crucial component of the thermal management systems PCMs absorb heat generated during battery operation, thereby enhancing battery performance, and extending battery lifespan [6].

Air cooling is widely regarded as the most convenient method extensively utilized in commercial applications. It significantly finds utility in EVs due to its cost-effectiveness, extended life span, easy maintenance, lightweight in construction and absence of leakage issues compared to other BTMS techniques used. Despite its numerous benefits air-cooling BTMS offers, it also presents various challenges, such as limited heat capacity and difficulties in ensuring uniform air distribution for consistent thermal performance in contrast to other methods. A considerable number of electric vehicles integrate air-cooling systems, employing either natural convection or induced convection methods. Natural cooling technique proves insufficient in high temperature environments, with larger battery packs, or during rapid charging and discharging cycles. To overcome this, induced convection methods such as blowers, ventilation systems, optimized ducts for airflow, and specialized fin arrangements have been devised. The battery packs in the EVs are generally uniformly packed and as the vehicle moves forward, external air enters through the openings on one side, flows correspondingly through the cells and finally exits through the openings on the opposite side, effectively dissipating the heat. Enhancing the air flow using fans or blowers becomes crucial, especially during slow vehicle movement or under high temperature conditions. BTMS incorporates active cooling components like fans, channels and turbines aids in ventilating surplus heat and maintaining consistent temperature distribution [9].

Metal foams represent a class of porous materials characterized by their low density and unique thermal and mechanical properties. The metal foams are generally classified into open-cell and closed-cell varieties. Open-cell type metal foams find extensive applications in heat exchangers. This foam is quite popular due to its elevated thermal conductivity, higher specific surface area and convoluted flow path which enhances mixing. The key properties of the metal foams which are extensively considered for the purpose of enhancement in the cooling by the researchers include permeability, thermal conductivity, and inertial coefficient [10]. Investigating the effective thermal conductivity, inertial coefficient and permeability of highly porous metal foams, Bhattacharya et al. designed a theoretical method. Their analysis highlighted the significance of porosity and the ratio of fiber cross-sections to intersections in determining effective thermal conductivity, with no clear relationship found with pore density. Fluid flow experiments unveiled a correlation between permeability and both pore diameter and medium porosity, while the inertial coefficient was found to be solely influenced by porosity. To predict the inertial coefficient and enhance the understanding of

permeability, the researchers proposed the theoretical and modified models, both validated through experimental results [11].

The main objective of this study is to employ a numerical approach, utilizing a 3-D model of a lithium- based battery of cylindrical shape. The model integrates metal foams with varying geometrical parameters saturated with air to facilitate thermal cooling of the batterie. Specifically, the investigation focuses on cooling dynamics during the discharge process under two specific C-rates of 0.5 and 1C respectively. GRG algorithm is utilized to estimate the change in internal resistance with temperature.

2. REPRESENTATION OF PHYSICAL MODEL

This study revolves around a standard lithium-polymer based cylindrical battery designed for electric mobility. Thermal control management was achieved through numerical analysis using Ansys-Fluent software. The cylindrical batteries, featuring Lithium-manganese oxide composition, were housed within parallelopiped-shaped casings. These casings were fully filled with metal foams of diverse porosities. Adjacent to the batteries, convective tubes were placed which acted as channels for fluid flow, with water assumed to be maintained at a constant temperature of 293.15 K. This circulating liquid ensured consistent casing wall temperatures, thereby enhancing overall thermal control of the battery pack system. The convective tubes maintained a constant temperature at the walls throughout the experiment thereby making the system to be adiabatic in nature. The design of the system is employed using the finite volume analysis technique. The results are analyzed considering the maximum temperature attained by the surface as well as the whole battery system. The temperature acquired by the metal foams during the process of discharge of the battery is also considered.

In Figure 1(a), cylindrical batteries are displayed in red, whereas the channels for liquid flow are displayed in blue, and the remaining grey area around the batteries and tubes indicate the mixture of aluminum metal foams of different porosities and pore densities which are saturated with air for the purpose of cooling the batteries during the process of discharge. Although Figure 1(a) portrays a complete battery pack, this study focuses on a single battery module. Considering the system's symmetrical nature, a single battery module is chosen, as illustrated in Figure 1(b). The single module was further reduced to a quarter, as displayed in Figure 1(c) to reduce the computational costs during the simulation ensuring reliable results.

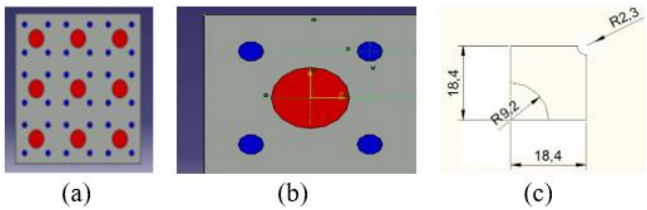

Figure 1. Battery pack arrangement and dimensions

2.1 Experimental analysis on estimation of internal resistance of battery cell

The experimental test bench methodology involved a Li-polymer based battery composed of lithium manganese oxide. Specifically, a cylindrical battery cell was selected for the experimental analysis, with model chosen being Efest: IMR18650. The specifications of the cell are tabulated in Table 1 [12, 13].

Table 1. Specifications of the battery

Properties	Specifications
Diameter [m]	0.184
Length [m]	0.0649
Weight [kg]	0.046
Capacity [Ah]	3.00
Maximum voltage [V]	4.2
Cut-off voltage [V]	2.5
c_p [kJ/kg K]	0.823
Density [kg/m^3]	2700
K [W/m K]	8.9

In this study, the thermal resistance of the battery cell in the model is analyzed over time. An experiment was conducted to assess the thermal resistance for a C-rate of 1C respectively. The C-rate of a battery refers to the time required for discharging and charging the battery within specific voltage limits [14]. The battery was connected to a programmable power supply which was serving both as a load and source depending upon the process. The module was further connected to a PC using an IEEE 488 GPIB bus.

During the process of discharge at a constant C-rate, the module served as a sink. The load settings and the battery's discharge were controlled remotely using Lab View software from National instruments. The programmable supply module was a KEPCO BOP 100-10MG. The experiment was initiated to charge the battery to a maximum voltage of 4.2 V. Further the battery was cooled until it reached room temperature. Subsequently, the battery was discharged with the two specific C-rates. Depending upon the chosen C-rates, the current was allowed to pass through the cell. The current and output voltage was measured using multimeters. The temperature of the cell was measured using a J-type thermocouple during the process of discharge and the time during the process was also recorded. The specifications of the module used in the experiment are displayed in Table 2 [12].

Table 2. Specifications of programmable power supply

Parameters	Specifications
Output voltage [V]	0 to ±100
Stabilizer	V/I 4-quadrant
Maximum power [W]	1000
Current accuracy	0.01% of rating
Output current [A]	0 to ±10
Switching frequency	100 KHz±5%

Moreover, the thermal resistance was assessed throughout the process of discharge correlating it with the depth of discharge. A non-linear exponential regression model was proposed by Zhang et al. [15] and Neumann and Lichte [16] and was chosen for the estimation of the internal resistance. The estimation of the internal resistance variation with respect to the temperature utilized the nonlinear GRG algorithm.

The algorithm was adopted utilizing the principles of curve fitting to the below mentioned equations of Eq. (1) to Eq. (3) respectively.

$$R(T) = R_0 \, exp \, b_1 T + b_2 T^2 \pm \gamma \quad (1)$$

$$V_{oc}(s) = K_0 - \frac{K_1}{s} + K_2 e^{-\alpha(1-s)} \quad (2)$$

$$V(t,T) = V_{oc}(s) - I(t) * R(T) \quad (3)$$

where, $V_{oc}(s)$ is the open-circuit voltage (OCV) of the battery which is a function of the state of charge of the battery given by s ∈ [0,1] in V [17], T corresponds to the temperature of the battery at that particular instant in K, R(T) represents the variable thermal resistance in ohm, γ denotes the offset parameter in mΩ, I represents the current flowing through the circuit in A, $V(t,T)$ is the terminal output voltage in V and K_0, K_1 and K_2 corresponds to the vector of model parameters, where the length of the K vector depends on the model and R_0 was assumed as 0.01Ω the series internal resistance of the battery.

The linear regression method was adopted to frame the relation between the internal resistance of the battery with respect to the depth of discharge of the battery cell [2, 18].

2.2 Mathematical formulation of the model

There are few assumptions based on which the model is designed. The various assumptions adopted in the model are listed below in detail:

i). The metal foams chosen for the thermal cooling process are isotropic and homogeneous.

ii). Heat transfer by means of radiation is neglected.

iii). The air saturating the metal foams obeys Boussinesq's approximation.

iv). The thermophysical properties of the constituents used in the thermal cooling process are assumed constant and the temperature is assumed to be ambient at initial condition.

The various mathematical equations governing the system during the process of heat transfer is presented below in detail [19-22]:

The equation of continuity influencing the motion of flow during the process is given by Eq. (4).

$$\frac{\partial u}{\partial x} + \frac{\partial v}{\partial y} + \frac{\partial w}{\partial z} = 0 \quad (4)$$

The equation of momentum influencing the motion of flow during the process is given by Eq. (5) to Eq. (7) respectively.

$$\frac{\rho_f}{\varepsilon}\left(\frac{\partial u_f}{\partial t} + \frac{u_f}{\varepsilon}\frac{\partial u_f}{\partial x} + \frac{v_f}{\varepsilon}\frac{\partial u_f}{\partial y} + \frac{w_f}{\varepsilon}\frac{\partial u_f}{\partial z}\right) = -\frac{\partial p_f}{\partial x} + \frac{\mu_f}{\varepsilon}\left(\frac{\partial^2 u_f}{\partial x^2} + \frac{\partial^2 u_f}{\partial y^2} + \frac{\partial^2 u_f}{\partial z^2}\right) + S_x \quad (5)$$

$$\frac{\rho_f}{\varepsilon}\left(\frac{\partial v_f}{\partial t} + \frac{u_f}{\varepsilon}\frac{\partial v_f}{\partial x} + \frac{v_f}{\varepsilon}\frac{\partial v_f}{\partial y} + \frac{w_f}{\varepsilon}\frac{\partial v_f}{\partial z}\right) = -\frac{\partial p_f}{\partial y} + \frac{\mu_f}{\varepsilon}\left(\frac{\partial^2 v_f}{\partial x^2} + \frac{\partial^2 v_f}{\partial y^2} + \frac{\partial^2 v_f}{\partial z^2}\right) + S_y \quad (6)$$

$$\frac{\rho_f}{\varepsilon}\left(\frac{\partial w_f}{\partial t} + \frac{u_f}{\varepsilon}\frac{\partial w_f}{\partial x} + \frac{v_f}{\varepsilon}\frac{\partial w_f}{\partial y} + \frac{w_f}{\varepsilon}\frac{\partial w_f}{\partial z}\right) = -\frac{\partial p_f}{\partial z} + \frac{\mu_f}{\varepsilon}\left(\frac{\partial^2 w_f}{\partial x^2} + \frac{\partial^2 w_f}{\partial y^2} + \frac{\partial^2 w_f}{\partial z^2}\right) + S_z \quad (7)$$

The various source terms in the momentum equation of the 3D model designed are formulated as given by Eq. (8) to Eq. (10).

$$S_x = \left(\frac{\mu_f}{K} + \frac{C_F}{\sqrt{K}}\rho_f \left|\vec{V_f}\right|\right) u_f \quad (8)$$

$$S_y = \left(\frac{\mu_f}{K} + \frac{C_F}{\sqrt{K}}\rho_f \left|\vec{V_f}\right|\right) v_f + \rho_f g \gamma_f (T_f - T_0) \quad (9)$$

$$S_z = \left(\frac{\mu_f}{K} + \frac{C_F}{\sqrt{K}}\rho_f \left|\vec{V_f}\right|\right) w_f \quad (10)$$

The energy equation involved with the motion of the saturated air embedded with the metal foam is expressed by Eq. (11).

$$\left(\rho_f c_{p,f}\right)_{eff}\left(u\frac{\partial T_f}{\partial x} + v\frac{\partial T_f}{\partial y} + w\frac{\partial T_f}{\partial z} + \frac{\partial T_f}{\partial t}\right) = k_{eff}\left(\frac{\partial^2 T_f}{\partial x^2} + v\frac{\partial^2 T_f}{\partial y^2} + w\frac{\partial^2 T_f}{\partial z^2}\right) \quad (11)$$

With regard to the source terms of the momentum equation, the initial term corresponds to the Darcy term where K here corresponds to the permeability of the metal foams and the next term refers to Forchheimer's term and C_F corresponds to the inertial resistance factor of the porous medium. The magnitude of $\vec{V_f}$ refers to the velocity of the fluid air during the process of thermal cooling. The second term in Eq. (9) corresponds to Bossiness's approximation. The various parameters related to the source term of the above equations are briefed down as follows. The inertial factor and the permeability are expressed by Eq. (12) and Eq. (13) respectively [11, 19].

$$C_F = 0.00212(1-\varepsilon)^{-0.132}\left(\frac{d_f}{d_p}\right)^{-1.63} \quad (12)$$

$$K = 0.00037(1-\varepsilon)^{-0.224}\left(\frac{d_f}{d_p}\right)^{-1.11} {d_p}^2 \quad (13)$$

where, the ligament diameter is expressed by Eq. (14) in m.

$$\frac{d_f}{d_p} = 1.18\sqrt{\frac{1-\varepsilon}{3\pi}}\left(\frac{1}{1 - e^{1(1-\varepsilon)/0.04}}\right) \quad (14)$$

where, the diameter of the pore is expressed by Eq. (15).

$$d_p = \frac{0.0254}{\omega} \quad (15)$$

The effective thermal conductivity and effective heat capacity involved in the energy equation is expressed by Eq. (16) and Eq. (17) respectively.

$$K_{eff} = A\left(\varepsilon K_f + (1-\varepsilon)K_s\right) + \frac{1-A}{\left(\frac{\varepsilon}{K_f} + \frac{1-\varepsilon}{K_s}\right)} \quad (16)$$

$$(\rho_f c_{p,f})_{eff} = \varepsilon(\rho_f c_{p,f}) + (1-\varepsilon)\rho_{mf} c_{mf} \quad (17)$$

where, u, v and w denote the velocities of flow in the x, y and z directions in m/s, p represents the relative pressure in N/m^2,

ρ_f refers to the density of the fluid air in kg/m^3, ε mentions about the porosity of the foam, γ_f refers to the thermal expansion coefficient and T_0 refers to the initial operating temperature in K. A is the traversal area of cross-section was assumed to be 0.35 and k_{eff} corresponds to effective thermal conductivity during the thermal process in W/m K and k_f and k_s refers to the fluid and solid thermal conductivities respectively.

The boundary conditions of the model are illustrated below as follows. The top and lateral surface of the battery was assumed to be adiabatic and symmetrical in nature which is expressed by Eq. (18):

$$\frac{\partial T}{\partial x} = 0, \frac{\partial T}{\partial y} = 0, \frac{\partial T}{\partial z} = 0 \tag{18}$$

The cooling liquid flowing through the tubes to maintain the constant temperature of the walls is expressed by Eq. (19):

$$T_{channel} = 293.15 \tag{19}$$

The temperature of the battery and the temperature of the metal foams saturated with air is assumed to be at identical temperatures at the surface of interface represented by Eq. (20).

$$T_{battery} = T_{mf} \tag{20}$$

From Eq. (20), it can be expressed that, the thermal transfer of heat in the model is identical between the metal foams and the battery module which is expressed by Eq. (21).

$$\dot{q}_{battery} = \dot{q}_{PCM} \tag{21}$$

Based on the above description of the boundary conditions and governing equations, the various specifications of the metal foams and saturated air used as fluid in the numerical model is displayed in Table 3 [11]. The specifications of the saturated air which is present along with the embedded metal foams inside the parallelopiped container is illustrated in Table 4 [19].

Table 3. Specifications of aluminium metal foams

Properties	Metal Foam (1)	Metal Foam (2)
ω [PPI]	20	40
ε	0.978, 0.9245	0.9272, 0.972
d_{fiber} [m]	0.000377, 0.000361	0.00025, 0.00023
d_{pore} [m]	0.00127, 0.00127	0.000635, 0.000635
C_f [m]	521.69, 535.27	773.722, 855.281
K [m^2]	8033076.36, 9037293.64	18359347.87, 19337443.19

Table 4. Saturated air specifications

Properties	Specifications
Density [kg/m^3]	1.225
c_p [J/kg K]	1006.4
Viscosity [kg/ms]	1.789e^{-5}
γ_f	0.00333
K [W/m K]	0.0242

2.3 Numerical model analysis

The physical model outlined above was addressed computationally using the Ansys-Fluent commercial code. The finite volume technique was applied to discretize and solve the model. The pressure-velocity coupling and pressure computations were resolved using the SIMPLE and PRESTO algorithms. A transient analysis utilized a time step of 0.1 s. Convergence was achieved with momentum and continuity errors limited to 10^{-5} and energy equation errors constrained to 10^{-8} [23].

A comparison among the four distinct meshes was conducted to determine the optimal accurate solution and simulation run time. These meshes were named sequentially as A, B, C and D respectively based on the count of elements comprising the mesh. Mesh D accounted for the maximum number of cells of 400,680. Mesh B comprised with a total number of 61,380 cells. Mesh C was made up of 108,108 cells and finally Mesh A accounted for 218,463 cells. On the application of grid independence test, the error percentage of the maximum temperature reached by the battery was estimated. From the analysis, it was estimated that Mesh C had an optimum solution as compared to other meshes. The grid independence test with the C-rate of 1C is displayed in Table 5.

Table 5. Grid independence test at C-rate=1C

Mesh	Maximum Temperature of Battery [K]	Maximum Temperature Error [%]
A	303.9091	0.0018
B	303.9166	0.0032
C	303.9126	-
D	303.9068	0.0007

3. RESULTS AND DISCUSSION

The key objective of this study was to estimate and analyze the peak surface temperature of the battery during the discharge process along with the average temperature of the metal foams of different porosities saturated with air. The maximum temperature of the entire battery along with the minimum temperature of the metal foam is also correspondingly noted for the purpose of analysis. The discharge process was carried out for a specific C-rate of 1C. Consequently, a numerical model was proposed and simulated to analyze the above-mentioned parameters using the Ansys Fluent software.

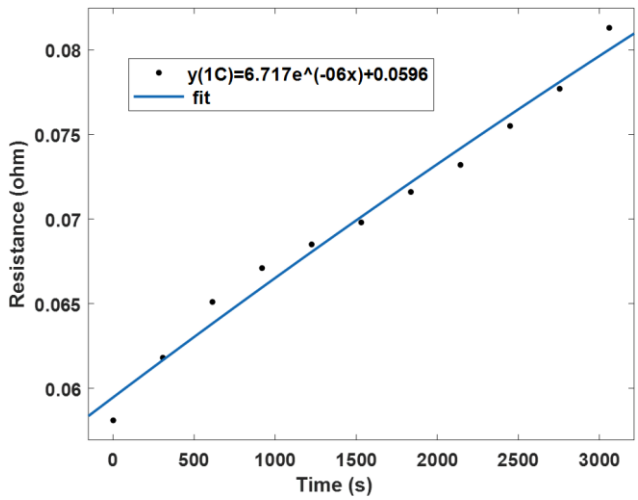

Figure 2. Regression analysis for C-rate = 1C

Based on the experimental analysis, the output-terminal voltage and the depth of discharge time were estimated for the discharge process at different C-rates. Additionally, by applying the Generalized Gradient Algorithm, a curve fit was performed to estimate the variable thermal resistance and open circuit voltage. A linear regression function was derived for these parameters concerning the depth of discharge for a C-rate of 1C as depicted in Figure 2, which was further applied in the numerical model analysis. The appropriate mesh was chosen based on the Grid independence test, and simulations were executed. The various parameters recorded for the metal foams of different porosities along with the battery are discussed below in detail.

The maximum temperature and surface temperature recorded by the battery during the process of discharge at 1C is illustrated below. Figure 3 displays the maximum temperature of the battery while Figure 4 shows the maximum surface temperature acquired by the battery surface during the process of discharge for a C-rate of 1C at two different pore densities and porosities.

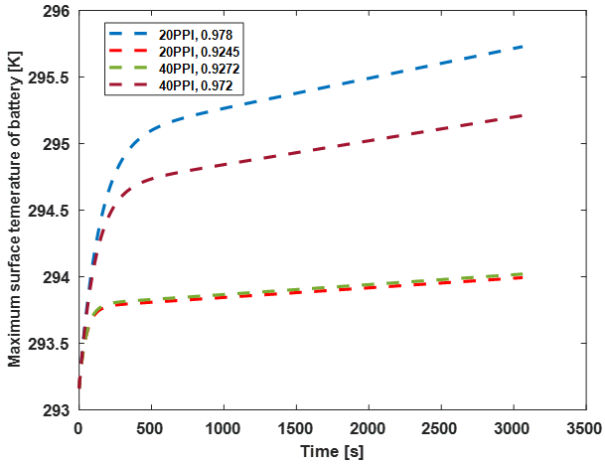

Figure 3. Characteristic response of maximum surface temperature on battery for different porosities

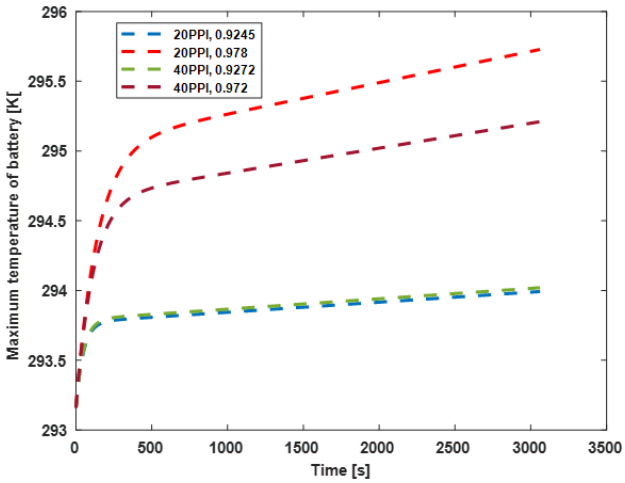

Figure 4. Characteristic response of maximum temperature on battery for different porosities

From the two characteristic responses, it is clearly observed that as the porosities decreases, the temperature acquired by the battery surface reduces. The metal foams embedded with air, with less porosities possess high thermal conductivity. Hence from the above figure, it is clearly observed that the metal foams with 40PPI pore density and 0.9272 has a lesser temperature both on the surface as well as the entire battery component. Moreover, the metal foams with 20PPI pore density and porosity equal to 0.978 displayed a high temperature among the four configurations.

The metal foams temperature which was acquired by them during the analysis is displayed in Figure 5 and Figure 6 respectively.

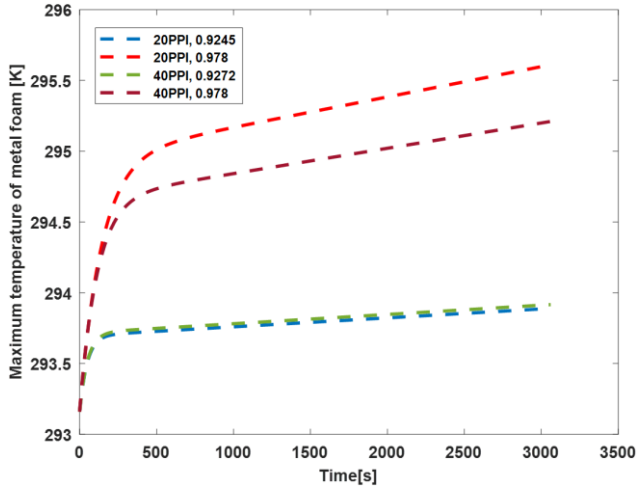

Figure 5. Characteristic response of maximum surface temperature on metal foams for different porosities

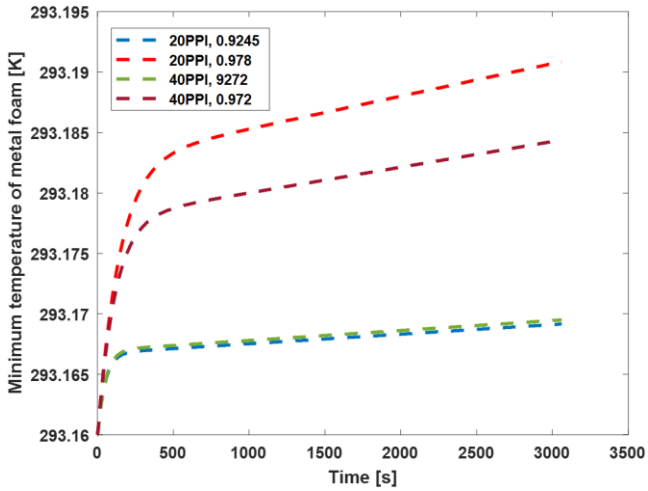

Figure 6. Characteristic response of minimum surface temperature on metal foams for different porosities

From the above two figures, it is clearly observed that they resemble the temperature profiles of the battery component. The metal foams with the highest pore density and the least porosity always provides a better characteristic reliability in the cooling of the battery. The metal foams with 40 PPI were performing relatively better in all the above cases, initiating form the maximum to the least temperatures both in the case of the battery as well as the metal foams which were placed embedded with the battery surface along with the saturated air. The porosities with the least configuration performed relatively much better in all the four cases with saturated air being the medium of heat transfer between the battery surface and the metal foams. The porosity equalling a value of 0.9272 in case of 40 PPI performed relatively the better among the different configurations. Followed by that was the metal foams with a pore density of 20 and pore density equalling a value of

0.9245. Among the configurations, the one which performed the least good was the configuration with 20 PPI pore density and porosity equalling a value of 0.978 respectively. Thus, from the above comparisons, it is clearly observed that the metal foams with high pore densities and least porosities performed relatively better in cooling of the batteries when saturated with air.

This study also supports the results proposed by Karkri [24], where the authors have used the metal foams along with phase change materials to have an appropriate heat transfer capability. From their results, it is observed that aluminium foam performed better than Nickel, but less than copper foams. Moreover, the metal foams with the maximum pore densities and least pore densities provided a better heat transfer property with the phase change materials to enhance the melting characteristics of the phase change materials thereby increasing the cooling and thereby bringing the temperature of the battery relatively lower as required by the system.

4. CONCLUSION

The study centered on the thermal analysis of lithium manganese oxide batteries at a specific C-rate of 1C respectively. An experimental procedure was employed to evaluate the changes in thermal internal resistance using the GRG algorithm and regression concepts. Additionally, a numerical model was developed using the Ansys-Fluent software. The battery system in the model included both active and passive cooling mechanisms, utilizing liquid cooling and metal foams embedded with saturated air. The model's outcomes were assessed for four parameters namely the maximum temperature of the whole battery component along with the maximum surface temperature acquired by the battery surface. Similarly, the maximum temperature acquired by the metal foams along with the minimum temperature acquired by the same embedded with saturated air. The metal foams used in the study were with two different pore densities and four different porosities. The metal foam with the highest pore density and the least porosity performed relatively better when compared with the different configurations for all the above-mentioned four parameters. This specific metal foam with higher pore density and least porosity performed better as they enhanced thermal conductivity of the saturated air and cooled down the battery relatively better than the other configurations. The study also suggests that exploring other hybrid cooling mechanisms could further enhance thermal behavior and performance of the battery systems.

ACKNOWLEDGMENT

This work was supported by the Italian Government MUR Grant No. P2022NYPHL – PRIN 2022 PNRR "VISIONS: eVolutIonary design of InnOvative heat traNsfer deviceS" – Funded by European Union – Next Generation EU.

REFERENCES

[1] Stan, A.I., Świerczyński, M., Stroe, D.I., Teodorescu, R., Andreasen, S.J. (2014). Lithium ion battery chemistries from renewable energy storage to automotive and back-up power applications—An overview. In 2014 International Conference on Optimization of Electrical and Electronic Equipment (OPTIM), Bran, Romania, pp. 713-720. https://doi.org/10.1109/OPTIM.2014.6850936

[2] Arumugam, A., Buonomo, B., Luiso, M., Manca, O. (2023). Lumped capacitance thermal modelling approaches for different cylindrical batteries. International Journal of Energy Production and Management, 8(4): 201-210. https://doi.org/10.18280/ijepm.080401

[3] Morris, M., Tosunoglu, S. (2012). Comparison of rechargeable battery technologies. In 2012 ASME Early Career Technical Conference, Atlanta, Georgia USA.

[4] Dell, R.M. (2000). Batteries: Fifty years of materials development. Solid State Ionics, 134(1-2): 139-158. https://doi.org/10.1016/S0167-2738(00)00722-0

[5] Zhou, W., Upreti, S., Stanley Whittingham, M. (2011). Electrochemical performance of Al-Si-graphite composite as anode for lithium-ion batteries. Electrochemistry Communications, 13(2): 158-161. https://doi.org/10.1016/j.elecom.2010.12.001

[6] Khan, A., Yaqub, S., Ali, M., Ahmad, A.W., et al. (2024). A state-of-the-art review on heating and cooling of lithium-ion batteries for electric vehicles. Journal of Energy Storage, 76: 109852. https://doi.org/10.1016/j.est.2023.109852

[7] Liu, H., Wei, Z., He, W., Zhao, J. (2017). Thermal issues about Li-ion batteries and recent progress in thermal battery thermal management systems: A review. Energy Conversion and Management, 150: 304-330. https://doi.org/10.1016/j.enconman.2017.08.016

[8] Kumar, P., Chaudhary, D., Varshney, P., Varshney, U., Yahya, S.M., Rafat, Y. (2020). Critical review on battery thermal management and role of nanomaterial in heat transfer enhancement for electrical vehicle application. Journal of Energy Storage, 32: 102003. https://doi.org/10.1016/j.est.2020.102003

[9] Nazar, M.W., Iqbal, N., Ali, M., Nazir, H., Amjad, M.Z.B. (2023). Thermal management of Li-ion battery by using active and passive cooling method. Journal of Energy Storage, 61: 106800. https://doi.org/10.1016/j.est.2023.106800

[10] Nawaz, K., Bock, J., Dai, Z., Jacobi, A.M. (2010). Experimental studies to evaluate the use of metal foams in highly compact air-cooling heat exchangers. In International Refrigeration and Air Conditioning Conference, p. 1150.

[11] Bhattacharya, A., Calmidi, V.V., Mahajan, R.L. (2002). Thermophysical properties of high porosity metal foams. International Journal of Heat and Mass Transfer, 45(5): 1017-1031. https://doi.org/10.1016/S0017-9310(01)00220-4

[12] Arumugam, A., Cipolletta, G., Delle Femine, A., Gallo, D., Landi, C., Luiso, M. (2022). Comparative analysis and validation of basic battery models for electric vehicles applications. In 2022 IEEE 12th International Workshop on Applied Measurements for Power Systems (AMPS), Cagliari, Italy, pp. 1-6. https://doi.org/10.1109/AMPS55790.2022.9978895

[13] Index of tested LiIon batteries. (2017). Efest IMR18650 3000mAh (Purple) 2017. https://lygte-info.dk/review/batteries2012/Efest%20IMR18650%203000mAh%20(Purple)%202017%20UK.html.

[14] Klein, R., Chaturvedi, N.A., Christensen, J., Ahmed, J., Findeisen, R., Kojic, A. (2013). Electrochemical model

based observer design for a lithium-ion battery. IEEE Transactions on Control Systems Technology, 21(2): 289-301. https://doi.org/10.1109/TCST.2011.2178604
[15] Zhang, C., Jiang, J., Zhang, L., Liu, S., Wang, L., Loh, P.C. (2016). A generalized SOC-OCV model for lithium-ion batteries and the SOC estimation for LNMCO battery. Energies, 9(11): 900. https://doi.org/10.3390/en9110900
[16] Neumann, D.E., Lichte, S. (2011). A multi-dimensional battery discharge model with thermal feedback applied to a lithium-ion battery pack. Modeling & Simulation, Testing and Validation (MSTV) Mini-Symposium.
[17] Pillai, P., Sundaresan, S., Kumar, P., Pattipati, K.R., Balasingam, B. (2022). Open-circuit voltage models for battery management systems: A review. Energies, 15(18): 6803. https://doi.org/10.3390/en15186803
[18] Arumugam, A., Buonomo, B., D'Arienzo, C., Romano, P., Manca, O. (2023). A numerical study on thermal control of batteries by phase change materials with liquid cooling. Journal of Physics: Conference Series, 2648(1): 012043. https://doi.org/10.1088/1742-6596/2648/1/012043
[19] Buonomo, B., Ercole, D., Manca, O., Menale, F. (2018). Thermal cooling behaviors of lithium-ion batteries by metal foam with phase change materials. Energy Procedia, 148: 1175-1182. https://doi.org/10.1016/j.egypro.2018.08.024
[20] Arumugam, A., Buonomo, B., Romano, P., Manca, O. (2024). Numerical investigation on liquid cooling of batteries in phase change materials. Journal of Physics: Conference Series, 2766(1): 012050. https://doi.org/10.1088/1742-6596/2766/1/012050
[21] Buonomo, B., Ercole, D., Manca, O., Nardini, S. (2016). Thermal behaviors of latent thermal energy storage system with PCM and aluminum foam. International Journal of Heat and Technology, 34(2): 359-364. https://doi.org/10.18280/ijht.34S224
[22] Buonomo, B., Manca, O., Nardini, S., Plomitallo, R.E. (2024). Numerical study on phase change material with metal foam in shell and convergent/divergent tube thermal energy storage systems with external heat losses. International Journal of Heat and Technology, 42(1): 1-9. https://doi.org/10.18280/ijht.420101
[23] Ansys-Fluent. (2018). Computational fluid dynamic code version 19.2 user guide. https://www.ansys.com/products/fluids/ansys-fluent.
[24] Karkri, M. (2019). A numerical investigation of the effects of metal foam characteristics and heating/cooling conditions on the phase change kinetic of phase change materials embedded in metal foam. Journal of Energy Storage, 26: 100985. https://doi.org/10.1016/j.est.2019.100985

NOMENCLATURE

Al	aluminium metal
BTMS	battery thermal management system
C- rate	time required to charge or discharge
DOD	depth of discharge
EV	electric vehicles
GRG	generalized reduced gradient algorithm
LTE	local thermal equilibrium
Li-ion	lithium- ion
OCV	open circuit voltage
PPI	pores per inch
A_{mush}	mushy zone constant
C_f	inertial drag coefficient, m
c_p	specific heat capacity, kJ/kg K
d_{fiber}	diameter of the fiber, m
d_{pore}	diameter of the pore, m
g	acceleration due to gravity, m/s^2
I	flowing current, A
K	permeability, m^2
K_0, K_1 and K_2	vector model parameters
p	relative pressure, N/m^2
q	thermal heat transfer, J/m^2 s
$R(T)$	variable thermal resistance, Ω
R_0	internal resistance, Ω
s	state of charge of battery
S	source term, N/ m^3
t	time instant, s
T	temperature of battery, K
u, v and w	velocity in x, y and z directions, m/s
$V_{oc}(s)$	open-circuit voltage, V
$V(t,T)$	terminal output voltage, V

Greek symbols

γ	offset parameter, mΩ
ω	pore density, PPI
ε	porosity of metal foam
μ	dynamic viscosity, kg. m^{-1}s^{-1}

Subscripts

oc	open circuit